0 0 0 0 4 3 0 5 2 8 9

LBL-3914
c.1

RECEIVED
LAWRENCE
BERKELEY LABORATORY

AUG 13 1975

LIBRARY AND
DOCUMENTS SECTION

DEFORMATION BEHAVIOR OF AN IDEALIZED CRYSTAL

Sabri Altintaş
(M. S. thesis)

May 1975

Prepared for the U. S. Energy Research and
Development Administration under Contract W-7405-ENG-48

For Reference

Not to be taken from this room

LAWRENCE BERKELEY LABORATORY
UNIVERSITY OF CALIFORNIA
BERKELEY

LBL-3914
c.1

DISCLAIMER

This document was prepared as an account of work sponsored by the United States Government. While this document is believed to contain correct information, neither the United States Government nor any agency thereof, nor the Regents of the University of California, nor any of their employees, makes any warranty, express or implied, or assumes any legal responsibility for the accuracy, completeness, or usefulness of any information, apparatus, product, or process disclosed, or represents that its use would not infringe privately owned rights. Reference herein to any specific commercial product, process, or service by its trade name, trademark, manufacturer, or otherwise, does not necessarily constitute or imply its endorsement, recommendation, or favoring by the United States Government or any agency thereof, or the Regents of the University of California. The views and opinions of authors expressed herein do not necessarily state or reflect those of the United States Government or any agency thereof or the Regents of the University of California.

0 0 0 0 4 3 0 5 2 9 0

DEFORMATION BEHAVIOR OF AN IDEALIZED CRYSTAL

Contents

ABSTRACT v

I. INTRODUCTION 1

II. STATISTICAL ANALYSIS 3

III. NUMERICAL ANALYSIS 12

A. Simulation Procedures 14

B. Simulation Results 16

1. Glide Velocity 16

2. Deformation of an Idealized Crystal 20

3. Stress-Strain Rate Relation 24

4. Flow Stress-Temperature Relation 25

IV. DISCUSSION 27

V. CONCLUSIONS 29

ACKNOWLEDGEMENTS 30

REFERENCES 31

FIGURE CAPTIONS 33

FIGURES 35

0 0 0 0 4 3 0 5 2 9 1

DEFORMATION BEHAVIOR OF AN IDEALIZED CRYSTAL

Sabri Altintaş

Inorganic Materials Research Division, Lawrence Berkeley Laboratory and
Department of Materials Science and Engineering, College of Engineering
University of California, Berkeley, California

ABSTRACT

The deformation behavior of an idealized crystal made by stacking of parallel slip planes is studied. Each slip plane is assumed to contain active sources of dislocations leading to a constant density of non-interacting dislocations in the plane which glide through randomly distributed localized point obstacles, representing small precipitates. The dislocation is assumed to have a constant line tension and the dislocation-obstacle interaction is taken to have a simple step form.

Using results of computer simulation of thermally activated glide through random arrays of point obstacles the deformation is modeled as a function of temperature and applied stress, determining the strain rate and the morphological characteristics of slip. Stress-strain rate and flow stress-temperature relations are discussed.

I. INTRODUCTION

The plastic deformation of a typical crystal is accomplished through the motion of dislocations. The available experimental data indicates that at moderate temperatures the dominant form of dislocation motion is planar glide, which is impelled by the local value of the resolved shear stress and opposed by the resistance of the microstructure. The dominant impediment to dislocation glide is often due to local microstructural features such as small precipitates, "forest" dislocations, or solute atoms which act as local barriers to dislocation motion.[1] The possibility of regulating the density, distribution or character of these barriers through the processes of alloying, irradiation and thermal and mechanical treatment provides a variety of methods to strengthen crystalline materials.[2-3] When these barriers are spread diffusely through the lattice they may often be regarded as point barriers in an approximately random distribution.

In the past several investigators used various experimental methods to study the velocity of individual dislocations.[3-5] Also a number of theories which treat the motion of dislocations in crystals containing barriers have appeared.[6-12] Most theories are based on the idea that the dislocations overcome the barriers by a thermally activated process and involve a number of simplifications.

Under suitable assumptions the problem of thermally activated dislocation glide through a field of point barriers can be simulated for direct solution.[13-15] Morris and Klahn[12,15] have discussed how statistical analysis and computer simulation may be combined to yield an

essentially complete solution for the velocity of dislocation glide as a function of applied stress, the temperature, and the nature of the barriers. By adding an assumption on the distribution of mobile dislocations, the results may be extended to model deformation of a single crystal which is assumed to deform through simultaneous glide of non-interacting dislocations on adjacent slip planes.

Morris and Klahn[15] reported preliminary results of a simulation of the deformation of a simple crystal at constant strain rate. The results were interesting in that the crystal not only showed the anticipated trend of flow stress with temperature but also exhibited a characteristic shift in the morphology of deformation with temperature: low temperature deformation concentrated on well-defined slip planes which became less pronounced as the temperature was raised.

In this thesis, the plastic deformation of an ideal crystal made up of a stacking of slip planes is simulated. The slip planes contain randomly dispersed obstacles having roughly the properties expected of small dispersion or precipitate particles. Furthermore, each slip plane is assumed to contain active sources of dislocations leading to a constant density of non-interacting dislocations in the plane. The deformation is then modeled as a function of temperature and applied stress, determining the strain rate and the morphological characteristics of slip. The results are reported below. First, the basic equations governing thermally activated glide will be reviewed and then the simulation procedures will be described.

II. STATISTICAL ANALYSIS

The assumptions and basic equations governing thermally activated glide of a simple dislocation through a field of randomly-distributed point barriers were developed in detail in reference 12. They may be summarized as follows: Consider a plane of a body which is the glide plane of a dislocation. Let it contain a random distribution of microstructural berriers, which are represented as point obstacles to dislocation glide. The array is described by the statement that its points are randomly distributed and by a characteristic length

$$\ell_s = (a)^{1/2} \tag{1}$$

where a is the average area per point. The total area of the square array is

$$A = n \cdot (\ell_s)^2 \tag{2}$$

where n is the total number of points contained. We can non-dimensionalize the area by dividing through by the square of the characteristic length, so as to get

$$A^* = A/(\ell_s)^2 = n \tag{3}$$

and the edge length of the square area in dimensionless form is

$$\ell^* = (A^*)^{1/2} = n^{1/2} \tag{4}$$

Let a dislocation be introduced into the glide plane. We model the dislocation as a flexible, extensible string of constant line tension Γ, its energy per unit length, and Burger's vector of magnitude b, which is taken to lie in the plane. Any dependence of Γ on the orientation of the line or on the mutual interaction of segments of the line will be neglected.

Let a stress $\underset{\sim}{t}$ be applied to the body containing the glide plane. If the dislocation moves so as to sweep out area A_s under the action of this stress the work done is[8]

$$\delta W = \tau b \delta A_s \tag{5}$$

where τ is the resolved shear stress impelling glide

$$\tau = (\underset{\sim}{b} \cdot \underset{\sim}{t} \cdot \underset{\sim}{k}) b^{-1} \tag{6}$$

and $\underset{\sim}{k}$ is the normal vector to the plane. The dislocation is assumed to move freely unless pinned by obstacles.

The resolved shear stress can be written in dimensionless form as

$$\tau^* = \tau \ell_s b / 2\Gamma \tag{7}$$

Let the dislocation under the applied stress τ^* encounter a configuration of point obstacles denoted by i (Figure 1). Between two adjacent

impenetrable obstacles the dislocation will take the form of a circular arc of radius

$$R = \frac{\Gamma}{\tau b} \tag{8}$$

which can be written in dimensionless form

$$R^* = \frac{R}{\ell_s} = \frac{\Gamma}{\tau b \ell_s} = \frac{1}{2\tau^*} \tag{9}$$

If the distance between any two adjacent obstacles along (i) exceeds $2R^*$ or if the dislocation line anywhere intersects itself, then the configuration (i) is transparent to the dislocation and will be mechanically bypassed. If (i) is not transparent, its mechanical stability is governed by the strength of the dislocation-obstacle interaction.

The obstacles in this study are assumed to be identical, circularly symmetric, localized barriers to the dislocation whose effective range of interaction (d) is small compared to their mean separation (ℓ_s). They may hence be treated as point obstacles.[16] At the k-th obstacle on the i-th configuration the dislocation line forms the asymptotic angle ψ_i^k ($0 \leq \psi_i^k \leq \pi$) (Fig. 1). The force, F_i^k, that the dislocation exerts on the k-th obstacle is simply, from Fig. 1

$$F_i^k = 2\Gamma \cos(\tfrac{1}{2}\psi_i^k) \tag{10}$$

or in dimensionless form

$$\beta_i^k = \frac{F_i^k}{2\Gamma} = \cos(\tfrac{1}{2}\psi_i^k) \tag{11}$$

The dislocation-obstacle interaction is governed by a force-displacement relation,[16] $\beta(x/d)$, the effective dimensionless point force on the dislocation as it sweeps through (or folds around[17]) the obstacle. A non-transparent line configuration of obstacles constitutes a mechanically stable barrier to the glide of a dislocation under stress τ^* if $\beta_i^k < \beta_c$ for all obstacles k on i, where β_c is a critical pre-selected obstacle strength, or if $\beta_i < \beta_c$, where β_i is taken to be the maximum of the β_i^k. The smaller stress τ^* at which $\beta_i > \beta_c$ for all configurations within the array (i.e., $\beta_1 > \beta_c$ where β_1 is the minimum of β_i) is the critical resolved shear stress τ_c^*, and the dislocation line containing β_1 is the strongest configuration. When $\tau^* < \tau_c^*$ the dislocation will encounter the least one stable configuration within the array, and can glide only with the help of thermal activation.

The force-displacement relation, $\beta(x/d)$, depends on the details of interaction. For simplicity an interaction of simple step form is assumed with

$$\beta = \beta_c \qquad \text{when} \qquad 0 \leq x/d \leq 1$$
$$\beta = 0 \qquad \qquad \text{otherwise}$$

If configuration (i) is mechanically stable it must be passed by thermal activation. We ignore the possibility of thermally activated bow-out of the dislocation line between obstacles and require that the activation occur at an obstacle. The activation energy is proportional to the area in force-displacement diagram (Figure 2) and may be written in dimensionless form

$$g_i^k = u(\beta_c) - u(\beta_i^k) \tag{12}$$

where $u(\beta)$ is the dimensionless area under both the force-displacement curve and a horizontal line of height β. The activation barrier at the k-th obstacle on (i) is then

$$\Delta G^{*k}_i = 2\Gamma d\, g^k_i \tag{13}$$

or

$$\Delta G^{*k}_i/kT = \alpha(\beta_c - \beta^k_i) \tag{14}$$

where α is the "dimensionless reciprocal temperature"

$$\alpha = \frac{1}{T^*} = \frac{2\Gamma d}{kT} \tag{15}$$

and

$$g^k_i = \beta_c - \beta^k_i \tag{16}$$

for the dislocation-obstacle interaction of simple step form.

The residence time of the dislocation in configuration i is the time required for thermal activation past at least one obstacle on i. The expected value of the residence time is[12]

$$\langle t^*_i \rangle = \Lambda_i^{-1} \tag{17}$$

where t^* is the dimensionless time νt, ν is the mean frequency with which the dislocation attempts an obstacle (assumed constant), and Λ_i is the activation parameter

$$\Lambda_i = \sum_{k=1}^{N_i} P^k_i \tag{18}$$

Here the summation is taken over the N_i obstacles on i and

$$P_i^k = \exp[-\alpha\ g_i^k] \tag{19}$$

is the probability for thermal activation past the (i,k) barrier in one attempt. The probability that activation will occur first at an obstacle k on (i) is[12]

$$\eta(k,i) = \Lambda_i^{-1} \exp(-\alpha\ g_i^k) \tag{20}$$

In thermally activated glide the dislocation encounters a sequence of obstacle configurations as it moves through the array (Figure 3). These define the "glide path" (χ) of the dislocation. To compute the glide velocity, we assume that the glide is controlled by thermal activation in the sense that the time required for glide between successive stable configurations along χ is negligible compared to the time required for thermal activation past these configurations. If there are r stable configurations along a particular path χ through the array then the expected transit time of a dislocation along χ is

$$\langle t_\chi^* \rangle = \sum_{i=1}^{r} \Lambda_i^{-1} \tag{21}$$

Given that the dislocation may take any one of many available glide paths through the array, the expected transit time is

$$\langle t^* \rangle = \sum_\chi \mu_\chi \langle t_\chi^* \rangle \tag{22}$$

where μ_χ is the probability that the path χ is followed in a given trial. A variety of ways have been suggested to calculate the average velocity

of a dislocation;[13] such as from the total area swept through and the total time during motion; from the distance traveled by the end of a dislocation and the total time; and from the average area per activation event and the average expectation time. Here, the velocity of a glide dislocation is defined in a statistical sense only, but has the ergodic average[12]

$$\langle v^* \rangle = n^{1/2}/\langle t^* \rangle \tag{23}$$

where v^* is the dimensionless area swept out by the dislocation per unit time divided by its projected length, the edge length of the array.

The determination of the velocity of glide through a random array of point obstacles is complicated since the available glide paths change with the applied stress, and the relative probabilities of these paths change with temperature. The glide path becomes precisely defined only in the limit of very low or very high temperature (T^*) or when the applied stress is very close to the critical value (τ_c^*) for athermal glide through the array. When T^* is small or $\tau^* \sim \tau_c^*$ the dislocation tends to follow the "minimum-angle" path (χ_0) obtained under the constraint that the dislocations pass each configuration (i) by activating past the point k at which the angle ψ_i^k takes on its minimum value or equivalently, at which β_i^k takes on its maximum value, β_i. In the limit of very low temperatures ($T^* \to 0$) the velocity is given by the Arrhenius equation

$$\langle v^* \rangle = n^{1/2} \exp[-\alpha(\beta_c - \beta_1)] \tag{24}$$

and the glide velocity is determined by the time required for thermal

activation at the weakest point along the strongest configuration in the array, where β_1 is the minimum of the β_i, i.e., the maximum force on the most stable configuration encountered during glide.

In the limit of very high temperatures ($T^* \to \infty$) the glide path becomes a "random" path (χ_R) whose configurations are obtained through a random sequence of activation events. In this case the velocity is again governed by an Arrhenius equation, with pre-exponential and activation energy given by suitable weighted averages over the random configurations.[12] At intermediate temperatures the equation governing glide are more complex, and cannot easily be set in Arrhenius form.

Given a satisfactory analysis for planes of randomly distributed obstacles one may treat the plastic deformation of an idealized crystal modeled as a stacking of planes of the same type. The model requires an additional assumption on the distribution of dislocations over the glide planes. The simplest assumption, which we shall make in the following, is that each glide plane contains active sources of non-interacting dislocations so that the expected number of dislocations is the same for all planes and all times during steady state deformation. Morris and Klahn[15] termed this a "uniform" distribution of dislocations. Given a crystal made up of S parallel glide planes containing a uniform distribution of dislocations the steady state strain rate may be written in dimensionless form

$$\dot{\gamma}^* = (\rho b/\ell_S)\tilde{v}^* \tag{25}$$

Here ρ is the expected number of dislocations intersecting a dimensionless area perpendicular to the glide planes and $\tilde{v}^*$ is the average of the

expected glide velocity for the individual planes in the crystal

$$v^* = \frac{1}{S} \sum_{\ell=1}^{S} \langle v_\ell^* \rangle \tag{26}$$

with $\langle v_\ell^* \rangle$ the expected value for the glide velocity of the dislocations gliding in the ℓ-th plane and S is the total number of glide planes.

If the individual glide planes contain a finite number of obstacles, then there may be appreciable scatter in the expected velocity from one plane to another. This will be reflected in an inhomogeneity of the crystal deformation, which will tend to concentrate on those planes over which glide is easiest ($\langle v_\ell^* \rangle$ is largest). As will be shown below, this plane-to-plane variation in glide velocity becomes less pronounced as the temperature (T^*) is increased or as the stress (τ^*) is decreased. Hence crystal deformation becomes more uniform as stress is lowered at constant temperature or as temperature is raised at constant stress.

III. NUMERICAL ANALYSIS

Foreman and Makin[13] used computers for the first time in studying the glide of dislocations through random arrays of point obstacles and demonstrated the usefulness of computers in obtaining an accurate solution of this complex problem. The first code to simulate thermally activated glide of a dislocation was written by Klahn et al.[14] They simulated dislocation glide as a function of stress (τ^*), obstacle strength (β_c), and temperature (T^*) assuming a simple step form for the dislocation-obstacle interaction. Morris and Klahn[15] showed that fundamental theorems could be used to simplify the computational effort required in a simulation of thermally activated glide and give a precise statistical definition to the velocity obtained.

Several interesting details of the thermally activated cutting of localized obstacles by the dislocation are exposed in these computer simulated experiments. Within the limits of the simplifying assumptions the computerized experiments (described in references 15 and 19) give what is believed to be an accurate statistical representation of thermally activated dislocation glide through randomly distributed obstacles. Thus, the computer simulation serves a two-fold purpose: first, it provides a guide for formulating an analytical approach to the statistical treatment of the subject; secondly it furnishes a reference for checking the accuracy of analytical approximations that might be designed for the solution of the problem.

Given the statistics of dislocation glide through localized, randomly distributed point obstacles and assuming a dislocation-obstacle interaction of simple step form, the time required for the dislocation

to travel through the array can be calculated and thus the velocity of the dislocation as a function of stress, temperature and obstacle strength can be obtained. To study the behavior of a crystal made up of parallel glide planes each of which contain an expected number (n) of obstacles in a Poisson distribution we fixed the number of planes (10 in this study), the number of obstacles (10^3 or 10^4) and the obstacle strength (0.1 or 0.6). The results are reported below.

The dislocations were assumed uniformly distributed over the glide planes. Hence the dislocation density in equation (25) could be treated as an arbitrary constant and the steady state strain rate $\dot{\gamma}^*$ measured by the velocity $\tilde{v}^*$. This velocity may then be calculated as a function of temperature (T^*) and stress (τ^*) for given obstacle strength (β_c). For completeness, our simulation studies covered the whole range of temperature (T^*). In fact, the melting temperature of all real materials fall at $T^* < 10^{-1}$. Hence $T^* \sim 10^{-1}$ gives an upper limit to physically reasonable values of the dimensionless temperature.

To determine the strain rate $\dot{\gamma}^*$ the expected glide velocity $\langle v^* \rangle$ for each of the glide planes as a function of temperature and stress was found, and summed according to equation (26) to give the average glide velocity of the planes in the crystal, $\langle \tilde{v}^* \rangle$, which is a measure for the strain rate $\dot{\gamma}^*$ (equation 25). The glide velocities were calculated through direct computer simulation. The simulation code employed is a modification of that described in reference 15. Its procedure is essentially as follows.[19]

A. Simulation Procedures

Using a pseudo-random number generator the code first fills the area of a square of size n with a random distribution of points of density one. The array is assumed periodic across all boundaries. The code then introduces a dislocation across the lower boundary of the array and allows it to move forward until it contacts points of the array. The dislocation bows out between adjacent points in a circle of continuously changing radius. The bow-out is terminated by one of three limits:

a) First, the dislocation segment may bow-out to the equilibrium radius R^*, given by equation 9, without contacting any third obstacle or violating the conditions of mechanical equilibrium ($\psi > \psi_c$) at either of the adjacent obstacles. In this case the dislocation segment is recognized to be mechanically stable.

b) Second, the dislocation may bow to the extent that it violates the condition $\psi > \psi_c$ at one of the adjacent obstacles. In this case the dislocation is allowed to pass the obstacle, a new segment is defined by the obstacles adjacent to the bypassed obstacle and the bow-out process begun anew.

c) Third, the dislocation segment may contact a third obstacle during bow-out. In this case the segment is divided, and the stability of the new segments tested by allowing them to bow out in turn.

This process of bowing the dislocation between obstacles, defining new segments when obstacles are contacted, and passing obstacles when ψ falls below ψ_c is continued until a dislocation configuration is found in which all obstacles are connected by segments which have the

equilibrium radius R^* and the angles at all obstacles are greater than the critical angle ψ_c. The dislocation is finally tested for self-intersections, which, given the method of construction, must occur at some point other than at an obstacle. If there are self-intersections, the dislocation is joined at the point of intersection, and a new search is begun. If there are no intersections, the configuration is recognized to be mechanically stable.

Given a stable configuration, the code computes the angles ψ_i^k along it, and uses the assigned value of the thermal parameter, α, to compute the mean residence time according to equation (17). It then calls a random number and chooses an activation site according to the probability assignment given in equation (20). The chosen point is passed, and the code then initiates a new search to establish the next stable configuration. In this way a statistically chosen glide path is generated and a transit time is computed according to equation (21). By allowing several sequential passages the ergodic average of the transit time is estimated (equation 22) and the glide velocity $\langle v^* \rangle$ found.

In simulating deformation of a crystal in which several glide planes must be treated simultaneously over a range of stress and temperature it is tedious and expensive to carry out a full statistical computation of $\langle v^* \rangle$. Morris and Klahn[12] identified approximate techniques which appeared particularly promising for use at low-temperatures. In reference 15 these are specifically studied. The most promising is the minimal sequence approximation, which ignores the change in glide path with temperature and assumes that the glide path is reasonably well approximated by the "minimum angle" path, χ_0. This assumption greatly

simplifies the computational effort necessary in simulating glide. Since the path χ_0 is fixed by stress[12] a single computer simulation experiment at a given value of τ^* yields sufficient information to determine the glide velocity for glide along χ_0 through a particular array at any value of the temperature.

B. Simulation Results

The computer simulation studies reported in this section focus on four problems: 1) the glide velocity and the accuracy of the "minimal sequence approximation," 2) the deformation of an idealized crystal, 3) the dependence of flow stress on the temperature. Now, these will be discussed in turn.

1. Glide Velocity

As mentioned above, the glide velocity of a dislocation can be obtained with reasonable accuracy using the minimal sequence approximation. To check its validity over the whole range of temperature, we compare the glide velocity computed in the minimal sequence approximation to that obtained from stochastic treatment of thermal activation for the stress $\tau^* = 0.4$ and obstacle strength $\beta_c = 0.6$. The number of obstacles was taken to be 10^3 (Figure 4). As is apparent from Figure 4, where we have plotted the dimensionless velocity v^* (specifically, its negative natural logarithm) against the thermal parameter, $\alpha = 1/T^*$, for the minimal sequence approximation (dashed line) and for a statistically chosen path (data bars indicating results of four independent trials), the approximation yields a reasonable result for values of the temperature as high as 10^{-1}, which corresponds to the highest realistic value of T^* for a deformable metal (Cd at its melting point). We hence

employed the minimal sequence approximation to simplify the simulation of crystal deformation.

Figure 5 illustrates the results obtained from simulation of a 10^4 point array for obstacle strength $\beta_c = 0.1$ and stresses $\tau^* = 0.001$, 0.01, and 0.03, using the minimal sequence approximation. As we can see in the figure the velocity increases monotonically with temperature (T^*) and stress (τ^*). At low temperatures (α high) the $-\ln\langle v^*\rangle$ vs. α curve approximates a straight line indicating a simple Arrhenius relationship. At high temperatures, however, a downward concavity (very pronounced at high stresses) is observed as shown in the data exhibited in Figures 3 and 5.

Given the accuracy of the minimal sequence approximation, in the following it will be used as the basis of a discussion of the dependence of the glide velocity $\langle v^*\rangle$ on the temperature (T^*), stress (τ^*) and obstacle strength (β_c). From equations (18), (19) and (21) the expected value of the transit time $\langle t^*\rangle$ along the path (χ_0) may be written[15]

$$\langle t^*\rangle = \{1 + Q - R - T_1\} \exp[\alpha(\beta_c - \beta_1)] \tag{27}$$

where

$$Q = \sum_{i=2}^{r_0} \exp[-\alpha(\beta_i - \beta_1)]$$

$$= \frac{\sum_{i=1}^{r_0} \exp[\alpha(\beta_c - \beta_i)] - \exp[\alpha(\beta_c - \beta_1)]}{\exp[\alpha(\beta_c - \beta_1)]} \tag{28}$$

$$R = \sum_{i=2}^{r_0} T_i \exp[-\alpha(\beta_i - \beta_1)$$

$$= \frac{\sum_{i=1}^{r_0} T_i \exp[\alpha(\beta_c - \beta_i)] - T_1 \exp[\alpha(\beta_c - \beta_1)]}{\exp[\alpha(\beta_c - \beta_1)]} \tag{29}$$

$$T_i = 1 - \{1 + \sum_{k=2}^{N_i} \exp[-\alpha(\beta_i - \beta_i^k)]\}^{-1}$$

$$= \frac{\sum_{k=1}^{N_i} \exp[-\alpha(\beta_c - \beta_i^k)] - \exp[-\alpha(\beta_c - \beta_i)]}{\exp[\alpha(\beta_c - \beta_i)]} \tag{30}$$

where r_0 is the total number of stable configurations along the path $_0$, β_i is the largest value of the obstacle strengths β_i^k, and N_i is the number of obstacles in the i-th configuration.

Figure 6 illustrates the dependence of the series Q, R, and T_1 on temperature and stress. They all decrease as the temperature increases (α decreases). The series Q is the lead correction term giving the decrement in $\langle v^* \rangle$ (increment in $\langle t^* \rangle$) due to the fact that the dislocation must activate past stable configurations in addition to the strongest along X_0. The series T_i is the lead correction term giving the increment to $\langle v^* \rangle$ from the possibility of thermal activation at a point other than the weakest in a stable configuration. The parameter T_1 specifically measures this effect for the strongest configuration (i=1). The series R is the correction term giving the increment to v^* in configurations other than the strongest one.

To solve for the parameters Q, R and T_1 analytically, hence to estimate the velocity of dislocations in the minimal sequence approximation, it is necessary to predict the properties of the obstacle configurations encountered in glide along the minimum-angle path, now unavailable. However, a brief discussion on the dependence of Q, R and T_1 values on the stress, temperature and obstacle strength can be given. In reference 15, the expression (27) has a sign error in it (equation V.1) and dropping R lead the authors to unreasonable approximation for the glide velocity in limiting cases (equation V.7). Thus, it is necessary to incorporate the parameter R into the discussion of T^*, τ^* dependence of $\langle v^* \rangle$.

At very low temperatures (α arbitrarily large) the velocity $\langle v^* \rangle$ is given by an Arrhenius equation of the form

$$\langle v^* \rangle = n^{1/2} \exp[-\alpha'(\beta_c - \beta_1)] \tag{31}$$

As temperature increases (α decreases) the parameters (Q-R) and T_1 become significant and $\langle v^* \rangle$ deviates from the above equation. The direction of the deviation is determined by the relative magnitudes of (Q-R) and T_1.

At high temperatures, T_1 approaches zero and the term (Q-R) determines the velocity. At low temperatures, however, T_1 dominates and thus determines the velocity.

The dominant influence of stress on the velocity is through the strength β_1. As τ^* increases β_1 increases, which in turn causes an exponential increase in the glide velocity v^*. The value of Q and R decreases as stress increases and in the limit when τ^* is sufficiently

close to τ_c^* the array contains only one stable configuration and Q and R are identically zero. The series T_1 is almost independent of τ^*. The obstacle strength β_c appears explicitly in the exponential in equation (31). A change in β_c at fixed τ^* will cause the velocity $\langle v^* \rangle$ to undergo an exponential change in the opposite direction. The series T_1 is independent of β_c and the series Q and R increase as β_c increases, decreasing or increasing the velocity, respectively.

Another striking result[20] obtained from computer simulation studies is that the motion of a dislocation through a finite array of point obstacles is usually jerky, which is in qualitative agreement with the experimental results of Gilman and Johnson[4] obtained by etching LiF specimens. A few positions within the array efficiently pin the dislocation for times long compared to the transit times between the "strong" configurations. Consequently, the dislocation appears to jump almost discontinuously from one of these configurations to another. The degree of this "jerkiness" is principally determined by the temperature and decreases as temperature is raised. The jerkiness of the motion also tends to increase with applied stress, but stress is the dominant variable only when the temperature is very high, the obstacle strength is very low, or the stress is close to τ_c^*.

2. Deformation of an Idealized Crystal

Given the behavior of a dislocation moving through randomly distributed obstacles we define a crystal made up of ten parallel glide planes each of which contains an expected number (10^3) of obstacles in a Poisson distribution. The strength of the obstacles was fixed at 0.6, which theoretical work by Bacon, Kocks, and Scattergood[21] suggests will

approximate the effective strength of an "impenetrable" particle in the plane. The force-displacement relation was assumed to have a simple step form. The obstacles hence roughly represent small precipitates or dispersion particles in the glide plane. Their number, 10^3, was chosen to facilitate computation. A physically more realistic number would be in the range of 10^6.

Figure 7 illustrates the central results obtained from simulation of the deformation of an idealized crystal made up of ten parallel glide planes having area 10^3, a uniform distribution of non-interacting dislocations and a Poisson distribution of obstacles having strength $\beta_c = 0.6$, and an interaction function, $\beta(x/d)$, of simple step form. The figure shows the glide velocity (plotted as $-\ell n\langle v^*\rangle$) as a function of $\alpha(= 1/T^*)$ for four values of the applied stress, τ^*. The light curves show the data for each of the individual glide planes making up the crystal (taken in the minimal sequence approximation), the heavy line gives the resulting deformational velocity (v^*) for the crystal as a whole.

The glide velocities for the individual planes vary over a range which increases as the temperature is lowered or the stress is raised. The source of this scatter is straight-forward and may be easily seen from the expression for the glide velocity in the low temperature limit (equation 31)

$$\langle v^*\rangle = n^{1/2} \exp[-\alpha(\beta_c - \beta_1)]$$

When the reciprocal temperature α is large the velocity is quite sensitive to small plane-to-plane variations in the value of β_1, the maximum force exerted on the most stable configuration encountered in glide along the minimum angle path. This variation is illustrated in reference

15. In a finite array the variation is significant and tends to increase with the stress τ^*. As the temperature is raised the properties of the most stable configuration become less dominant. In the high temperature limit the glide velocity is determined by an average over the forces. Unless τ^* is so near τ_c^* that there are only a few stable configurations in the array this average tends to be independent of the specific array, and the variation of $\langle \tilde{v}^* \rangle$ becomes very small.

The plane-to-plane variation in glide velocity is enhanced by the small array size used in this simulation, 10^3, as opposed to a physically realistic number of perhaps 10^6. Were the array size increased the variation would become less pronounced. Specific simulations of very large arrays have, however, shown that the plane-to-plane variation remains significant when the number of obstacles is increased to 10^6 or more.

The consequences of the plane-to-plane variation in glide velocity are illustrated in Figure 8, where we show the appearance of a hypothetical tensile bar made of our model crystal and strained 20% in tension at each of two resolved shear stresses, $\tau^* = 0.01$ and $\tau^* = 0.04$, at tempera- $T^* = 10^{-3}$ and 10^{-1}. At low stress ($\tau^* = 0.01$) the deformation is markedly inhomogeneous at the lowest temperature ($T^* = 10^{-3}$), but rapidly becomes homogeneous as temperature is raised. At high stress ($\tau^* = 0.4$) the deformation remains inhomogeneous even at $T^* = 10^{-1}$, which roughly corresponds to the highest dimensionless temperature attainable in a typical metal.

A second salient qualitative feature of the data shown in Figure 7 concerns the possibility of representing the deformational velocity by

an Arrhenius equation. At low temperatures the velocity $\tilde{v}^*$ is given by an Arrhenius equation of the form

$$v^* = \left(\frac{n}{s}\right)^{1/2} \exp[-\alpha(\beta_c - \beta_{1m})] \tag{32}$$

where β_{1m} is the largest of the β_1 values for the s planes composing the crystal. However as T^* is increased (α decreased) $\tilde{v}^*$ deviates from equation (32) by an amount which represents a balance between the increasing contribution of glide on secondary planes and the increasing importance of secondary activation events in the primary glide plane. As discussed before, at intermediate temperatures $\tilde{v}^*$ tends to fall below the values predicted by the asymptotic relation (32), a result reflected in the light upward concavity of the curves at $\tau^* = 0.01$-0.25. However, as τ^* approaches τ_c^* this effect is reversed and $\tilde{v}^*$ tends to exceed the value predicted by equation (32), thus the downward concavity of the curve for $\tau^* = 0.4$. Note, however, that the data shown here span many orders of magnitude of $\tilde{v}^*$. Were we to confine the data to a range (5-10 orders of magnitude of $\dot{\gamma}^*$) which might be experimentally measurable, the data would be well fit by an Arrhenius equation at intermediate temperature.

At very high values of T^* (above the melting point of a plausible crystal in this specific example) a pronounced downward concavity is observed, as shown in the data exhibited in Figure 4. This phenomenon reflects the rapid increase in $\tilde{v}^*$ as the probable glide path of the dislocation changes from one dominated by the minimum angle path, χ_0, to the much easier glide paths which approach the random path, χ_R. The effect is a rapid thermal "softening" of the crystal, which has its

source entirely in the thermal choice of the glide path, the properties and distribution of obstacles remains the same.

The variation of slip morphology with stress at constant temperature is illustrated in Figure 9, where we have shown idealized tensile bars after a strain of 20% at four values of stress ($\tau^* = 0.01$ to $\tau^* = 0.4$) at $T^* = 10^{-2}$. The tendency of slip to become more inhomogeneous as stress is raised is apparent in the figure.

The change in slip morphology with temperature at constant strain rate ($\tilde{v}^*$) is illustrated in Figure 10. The results qualitatively reproduce those reported in reference 15. Deformation rapidly becomes homogeneous as T^* is raised, since both the increase in temperature and the decrease in flow stress favor homogeneous slip.

3. Stress-Strain Rate Relation

Figure 11 illustrates the variation of glide velocity with stress in tests conducted at constant temperature. In keeping with the conventional representation

$$\dot{\gamma}^* \sim (\tau^*)^{m*} \tag{33}$$

the data are plotted in logarithmic coordinates. The stress exponent m* is then the slope of the curve:

$$m* \equiv \frac{\partial \log \tau^*}{\partial \log \dot{\gamma}^*} \tag{34}$$

As is apparent from Figure 11 the data do not show a well-defined stress exponent. The parameter m* is a function of both τ^* and T^*. However,

again the data span many orders of magnitude of strain rate; were the data confined to a plausible experimental range a reasonably constant stress exponent would be obtained.

At low temperature ($T^* = 10^{-3}$) the value of m* is large and increases rapidly with stress, from a value of the order of 80 at $\tau^* = 0.01$ to a value above 300 at $\tau^* = 0.4$. As temperature increases both the stress exponent and its stress variation diminish. At $T^* = 10^{-2}$ the stress exponent is about 10 at low stress, increasing to $\sim$35 as stress approaches τ_c^*. At $T^* = 10^{-1}$ the stress exponent is near 1.0 at low stress, increasing about 10 near τ_c^* (Table 1.

4. Flow-Stress - Temperature Relation

Flow stress of a crystal is defined as the value of τ^* to sustain a constant strain rate $\tilde{v}^*$ in this model. We consider the variation of flow stress with the testing temperature. Since at low temperatures the velocity is given by an Arrhenius form (equation 31) the temperature dependence of the flow stress at constant strain rate can be written in the form

$$T^* = A - B(\tau^*)^{2/3} \tag{35}$$

where A and B are constants. The result depends on the precise value of $\tilde{v}^*$ chosen, when $T^* > 0$ the flow stress is an increased function of strain rate. Plots for two choices of $\tilde{v}^*$ are shown in Figure 12. The flow stress decreases monotonically from the value τ_c^* when $T^* = 0$. As expected the rate of decrease falls as the strain rate is raised. Since in this simple example there is no athermal component to the flow stress,

and since the maximum value of the activation barrier at an obstacle is finite, the flow stress becomes zero at a finite value of T^* which depends on strain rate and increases as v^* is raised. By extrapolation in Figure 12, τ^* vanishes for $T^* \gtrsim 3.5 \times 10^{-2}$ when $\ell n\langle v^*\rangle = -20$, and for $T^* \gtrsim 7.2 \times 10^{-3}$ when $\ell n\langle v^*\rangle = -10$.

IV. DISCUSSION

The computer simulation experiments discussed above give us information on the statistics of overcoming of local obstacles by dislocations which is needed for a reliable analysis of the experimental data and for the further development of the theory of dislocation mobility, and crystal plasticity. However, the results obtained are sensitive on the approximations used and it is necessary to check the validity of the assumptions and modifications of the model. Due to the lack of detailed knowledge concerning the density of obstacles, their strength, etc. in experiments on real materials a quantitative comparison at this stage is not possible.

We will now discuss briefly the validity of the assumptions: The assumption of randomness of point obstacles is a good one if the obstacles are non-interacting impurities, small dispersion particles or small voids. Interacting point obstacles or flexible forest dislocations will not be random. Obstacles were assumed to be point obstacles. In most models, the nature of obstacles has generally been unspecified, a proper description of point obstacle approximation is necessary. According to Morris and Syn,[16] if the effective range of interaction (d) is small compared to the mean separation (ℓ_s) of the obstacles which are taken to be identical circularly symmetric barriers to the dislocation glide, then the obstacles can be treated as point obstacles. Thus, in this model we are only concerned about barriers with short-range interaction. Line-like obstacles and obstacles of different size and spacing[22] and non-localized obstacles[10] have been treated in the literature. The nature of the motion of a dislocation through non-random obstacles can

of course be quite different.

Dislocations were assumed to be flexible, extensible strings of constant line tension, thus, neglecting effects of orientation, radius of curvature and the influence of elastic anisotropy on the energy of the dislocation. Bacon et al.[21] considered the change in line tension with dislocation type and obstacle spacing when the obstacles are strong. We also neglected the interactions between dislocation branches on either side of the obstacles, and interactions arising between dislocations on different slip planes.

A force-displacement diagram of simple step form was assumed. As indicated by Ono[23] the diagrams discussed in the literature fall into two classes: "calculated" and "intuitive." Very few attempts have been made to calculate force-displacement diagrams for particular local obstacles and these are restricted to the simpler elastic interactions.[24] Since the temperature dependence of the flow stress is very sensitive to the shape of the force-displacement diagram an agreement between experimentally determined temperature dependence of flow stress and that predicted by a theory is not necessarily unique.

V. CONCLUSIONS

The deformation behavior of an idealized crystal made by stacking of planes each of which contained non-intersecting dislocations and randomly distributed localized point obstacles is studied. Assuming a dislocation-obstacle interaction of simple step form and dislocations of constant line tension the following conclusions are made:

1) When the obstacle strength is large, the minimal sequence approximation yields a good estimate for the glide velocity over a wide range of temperature (see Figure 4). As discussed earlier, at low temperatures and high stresses the dislocation follows the minimum angle path χ_0 and the strongest configuration is strength determining. At moderate temperatures the difference between configurations diminishes.
2) The motion of dislocations is more discontinuous at low temperatures and low stresses. An idealized crystal made up of stacking of slip planes will show inhomogeneous behavior at low temperatures and high stresses, because the crystal deformation tends to concentrate on those planes on which glide is easiest.
3) The stress exponent, m^*, will depend both on temperature and stress and will increase as stress increases or temperature decreases. This suggests that velocity and stress cannot be set in simple proportionality.
4) The flow stress of an idealized crystal will decrease monotonically as temperature increases or strain rate decreases.

ACKNOWLEDGEMENTS

The author is indebted gratefully to Professor J. W. Morris, Jr. for his continuous guide and encouragement throughout this study. The thanks are also due to Kenton Hanson for his assistance in programming aspects of the problem and to Professors J. Washburn and F. E. Hauser or reviewing the manuscript.

This work was supported by the U.S. Energy Research and Development Administration through the Inorganic Materials Research Division of the Lawrence Berkeley Laboratory.

REFERENCES

1. J. Friedel, in Electron Microscopy and Strength of Crystals, G. Thomas and J. Washburn, eds. (J. Wiley, New York, 1963), p. 605.
2. A. Kelly and R. B. Nicholson, Strengthening Methods in Crystals (Applied Science Publishers, London, 1971).
3. A. R. Rosenfield, G. T. Hahn, A. L. Bement, Jr., and R. I. Jaffee, Dislocation Dynamics (McGraw-Hill, New York, 1968).
4. J. J. Gilman and W. G. Johnson, J. Appl. Phys. 30, 129 (1959).
5. T. Imura, in Electron Microscopy and Structure of Materials, G. Thomas et al., eds., University of California Press (1972), p. 104.
6. J. A. Simmons and R. Bullough, eds., Fundamental Aspects of Dislocation Theory, Nat. Bu. Std. Special Publication 317, Vol. I, Washington, D.C. (1970).
7. A. S. Argon, Phil. Mag. 25, 1053 (1973).
8. J. Friedel, Dislocations (Addison-Wesley, Reading, Mass., 1964).
9. J. E. Dorn, Dislocation Dynamics (McGraw-Hill, New York, 1968), p. 27.
10. F. R. N. Nabarro, J. Less Common Metals 28, 257 (1972).
11. U. F. Kocks, Phil. Mag. 13, 541 (1966).
12. J. W. Morris, Jr. and D. H. Klahn, J. Appl. Phys. 44, 4882 (1973).
13. A. J. E. Foreman and M. J. Makin, Phil. Mag. 14, 911 (1966); Canad. J. Phys. 45, 511 (1967).
14. D. Klahn, D. Austin, A. Mukherjee, and J. E. Dorn, in Advances in Applied Probability, Supplement 2 (1973), p. 112.
15. J. W. Morris, Jr. and D. H. Klahn, J. Appl. Phys. 45, 2027 (1974).
16. J. W. Morris, Jr. and C. K. Syn, J. Appl. Phys. 45, 961 (1974).

17. E. Orowan, Symposium on Internal Stresses, Inst. Metals, London (1947), p. 451.

18. S. I. Zaitsev and E. M. Nadgorvyi, Sov. Phys. Solid State 15, 1777 (1974).

19. S. Altintas, K. Hanson, and J. W. Morris, Jr., J. Materials and Technology (in press).

20. D. H. Klahn and J. W. Morris, Jr., in Rate Processes in Plastic Deformation, J. C. M. Li, ed. (Plenum, in press).

21. D. J. Bacon, U. F. Kocks, and R. D. Scattergood, Phil. Mag. 28, 1241 (1973).

22. A. J. E. Foreman, P. B. Hirsch, and F. J. Humphries, in Electron Microscopy and Structure of Materials, G. Thomas et al., eds., University of California Press (1972), p. 1083.

23. K. Ono, J. Appl. Phys. 39, 1803 (1968).

24. C. K. Syn, Ph.D. Thesis, University of California, Berkeley (1973).

FIGURE CAPTIONS

Figure 1. Configuration of a dislocation pressed against an array of obstacles by a stress τ.

Figure 2. (a) A possible force-displacement relation, $\beta(x/d)$, for dislocation passage through an obstacle which forms a simple repulsive barrier. The shaded area indicates the activation energy (g_i^k) if the dislocation exerts a force β_i^k on the obstacle.

(b) The assumed step form of the dimensionless dislocation-obstacle interaction, $\beta(x/d)$. The obstacle strength is β_c. The shaded area is g_i^k, the activation energy required when the dislocation exerts a force β_i^k on the obstacle.

Figure 3. Sequence of four possible configurations as a dislocation glides into a random array of point obstacles. The activation side is indicated by the symbol (Δ).

Figure 4. Comparison of the results using minimal sequence approximation (dashed line) and statistically chosen path. The data bars indicate results of four independent trials.

Figure 5. Results of a simulation of thermally-activated glide through an array of 104 obstacles, showing the average glide velocity $\langle v^* \rangle$ as a function of the thermal parameter α, at three stresses: $\tau^* = 0.001$, 0.01 and 0.03, with obstacle strength $\beta_c = 0.1$.

Figure 6. Q, R and T_1 values as a function of α at $\tau^* = 0.01$ and $\beta_c = 0.1$ for an 10^4 point array.

Figure 7. Comparison of the velocity-temperature relations for ten arrays of 10^3 obstacles having $\beta_c = 0.6$ at each of four stresses (light lines). Also included are the velocity-temperature curves for a crystal made up of these ten arrays under the assumption of a "uniform" distribution of dislocations over the planes (circles, heavy lines).

Figure 8. Illustration of the deformation of a hypothetical crystal made up of ten glide planes whose properties are shown in Figure 7. This figure shows the change in the appearance of the deformed crystal with temperature, assuming that the crystal contains a uniform distribution of dislocations of fixed density, and is given a total shear strain $\gamma = 20\%$.

Figure 9. Variation of slip morphology with stress at constant temperature. Idealized tensile bars are shown after a strain of 20% at four values of stress ($\tau^* = 0.01, 0.1, 0.25, 0.4$) at $T^* = 10^{-2}$.

Figure 10. Illustration of slip morphology with temperature at constant strain rate ($\ell n\langle\tilde{v}^*\rangle = -20$).

Figure 11. Illustration of the variation of glide velocity with stress in tests conducted at constant temperature. In this figure $\ell n\langle v^*\rangle$ is plotted against $\log \tau^*$ at constant temperature ($T^* = 10^{-3}, 10^{-2}, 10^{-1}$).

Figure 12. The variation of the flow stress with the testing temperature at constant strain rates ($\ell n\langle v^*\rangle = -10, -20$).

0 0 0 4 3 0 5 3 0 9

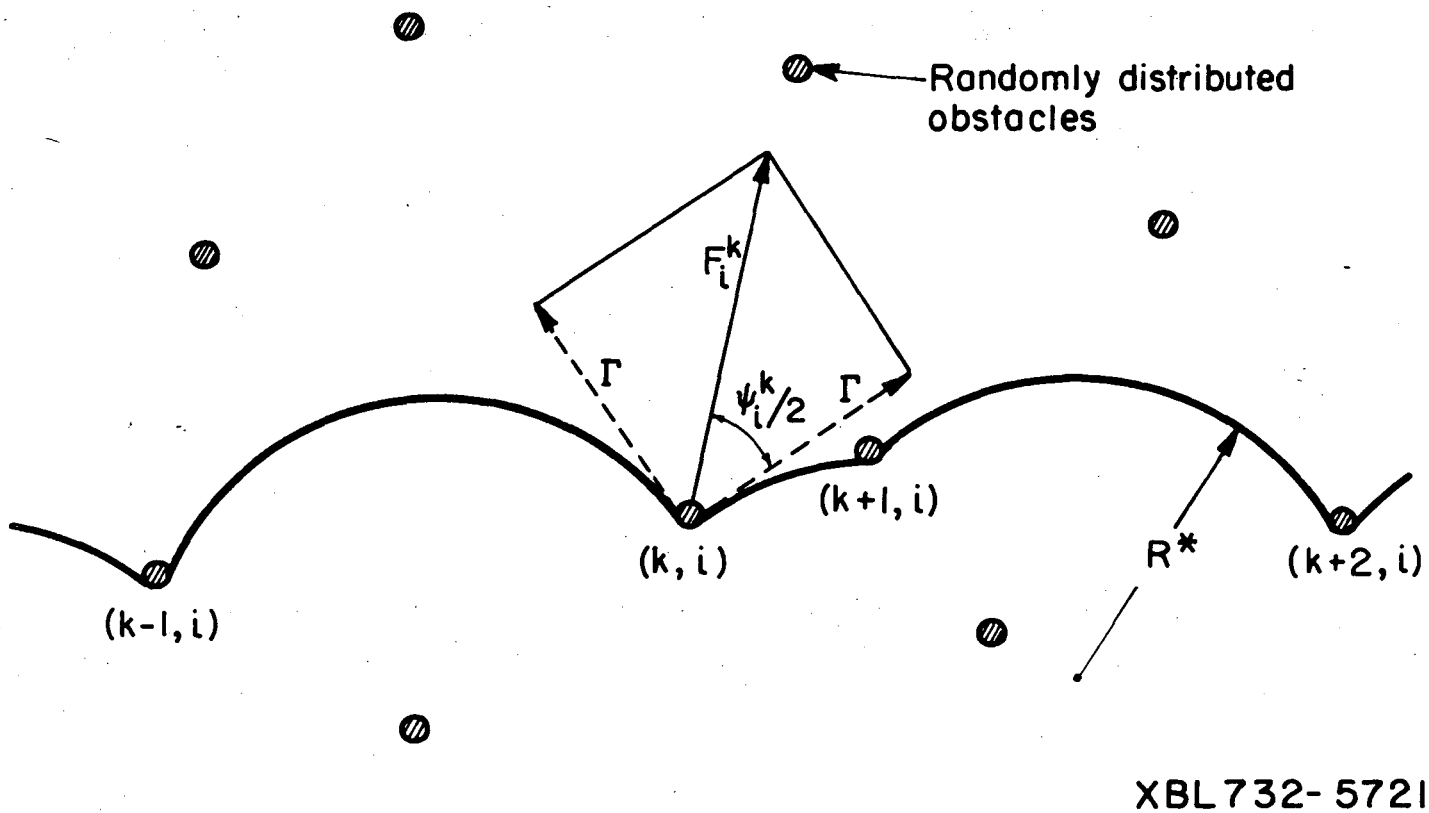

Fig. 1

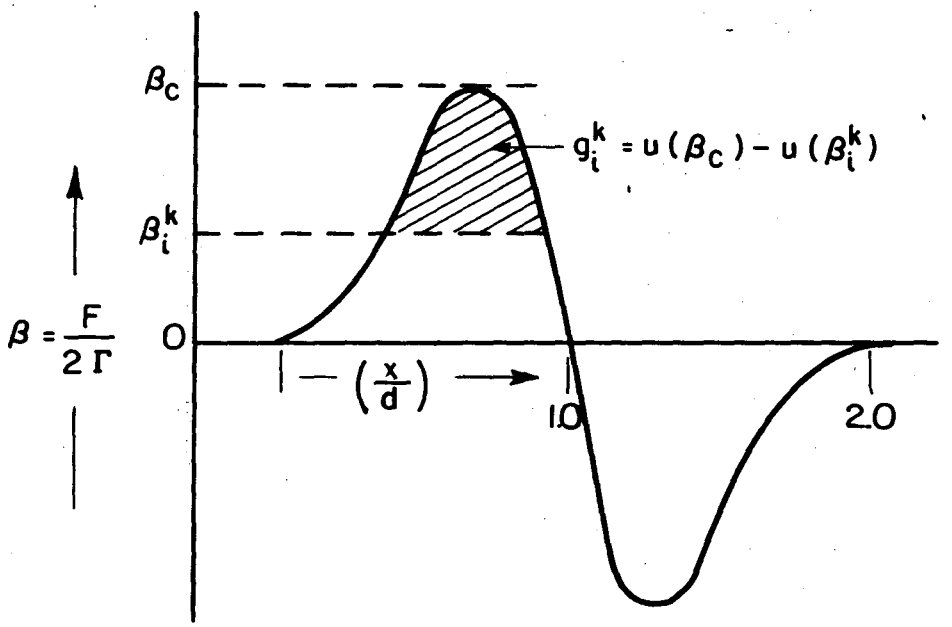

(a)

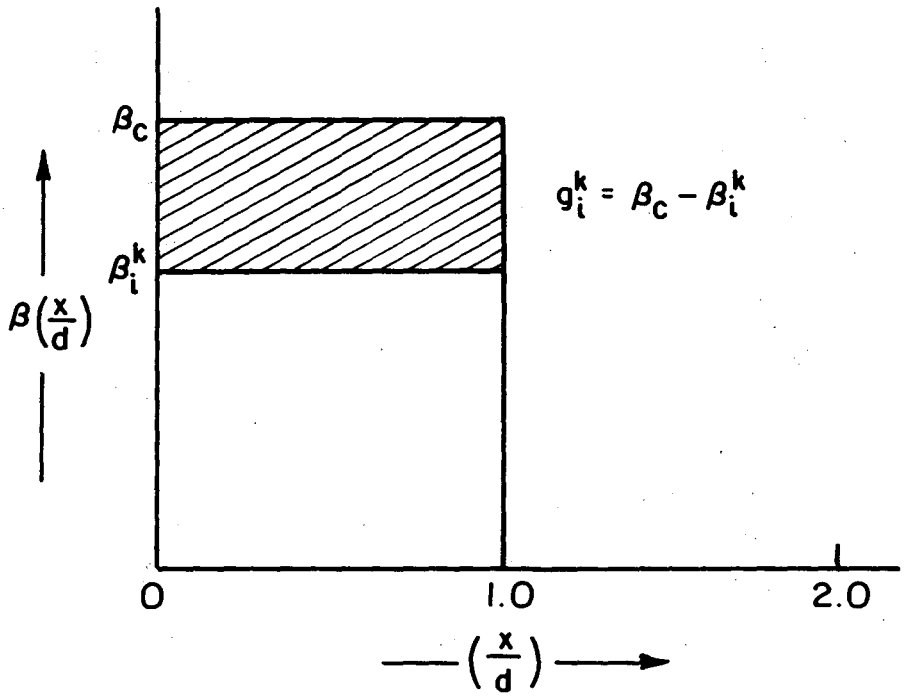

(b)

XBL 754-6131

Fig. 2

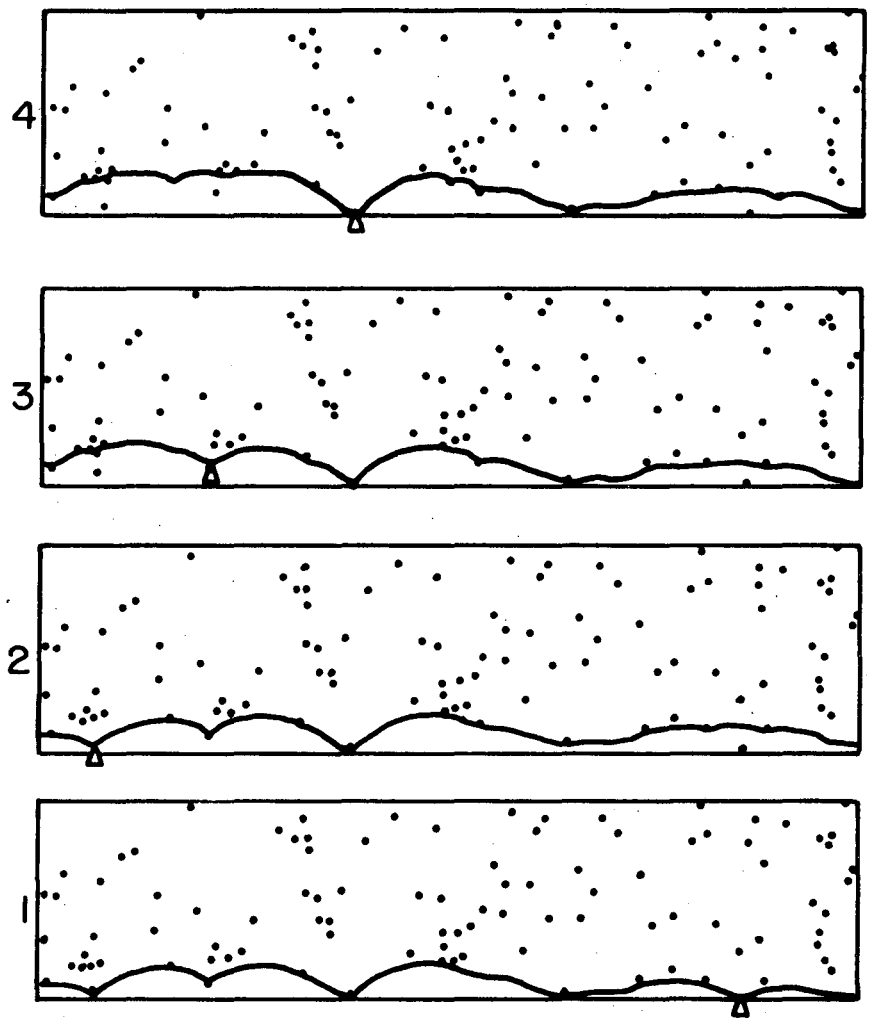

XBL732-5722

Fig. 3

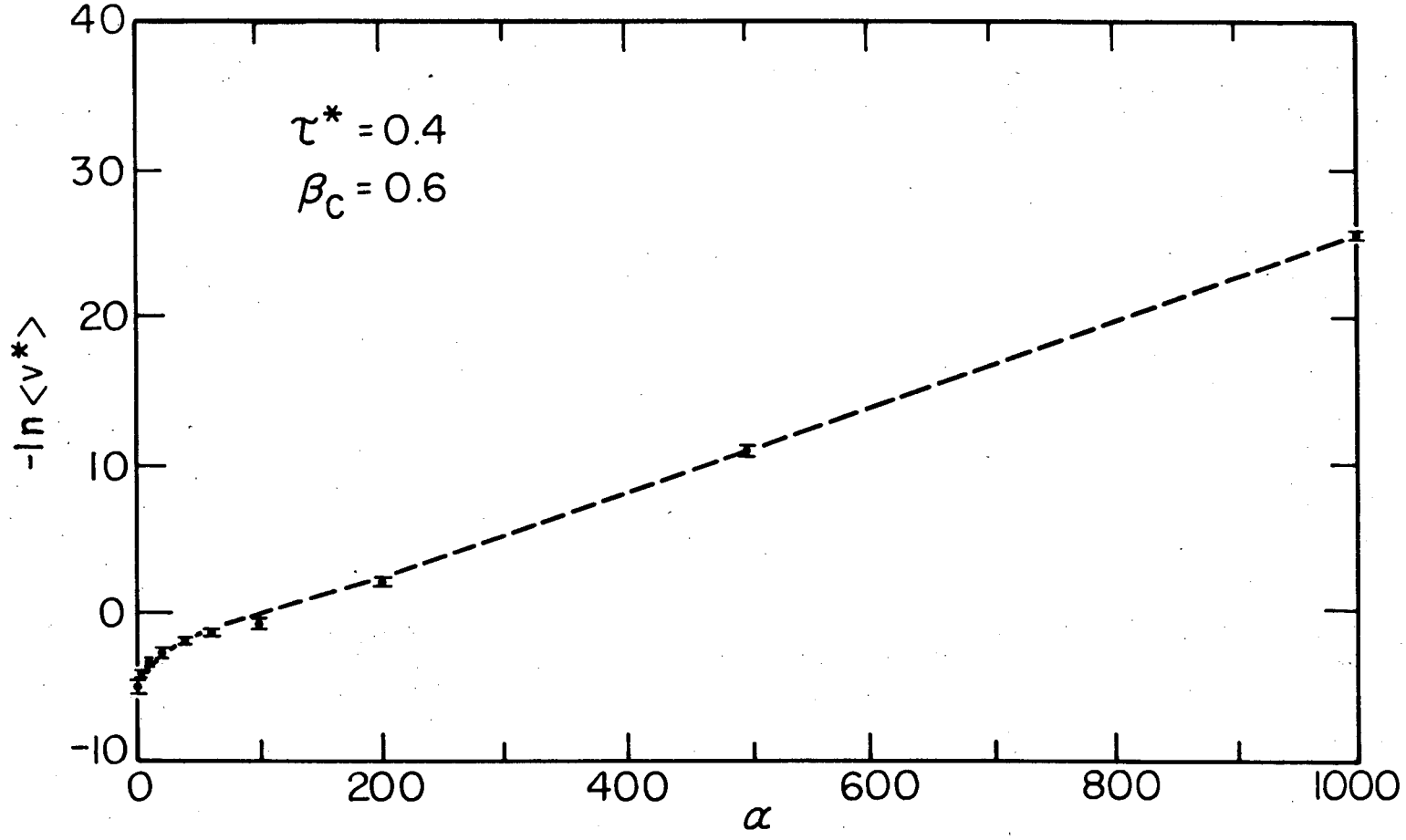

XBL 7410-7504

Fig. 4

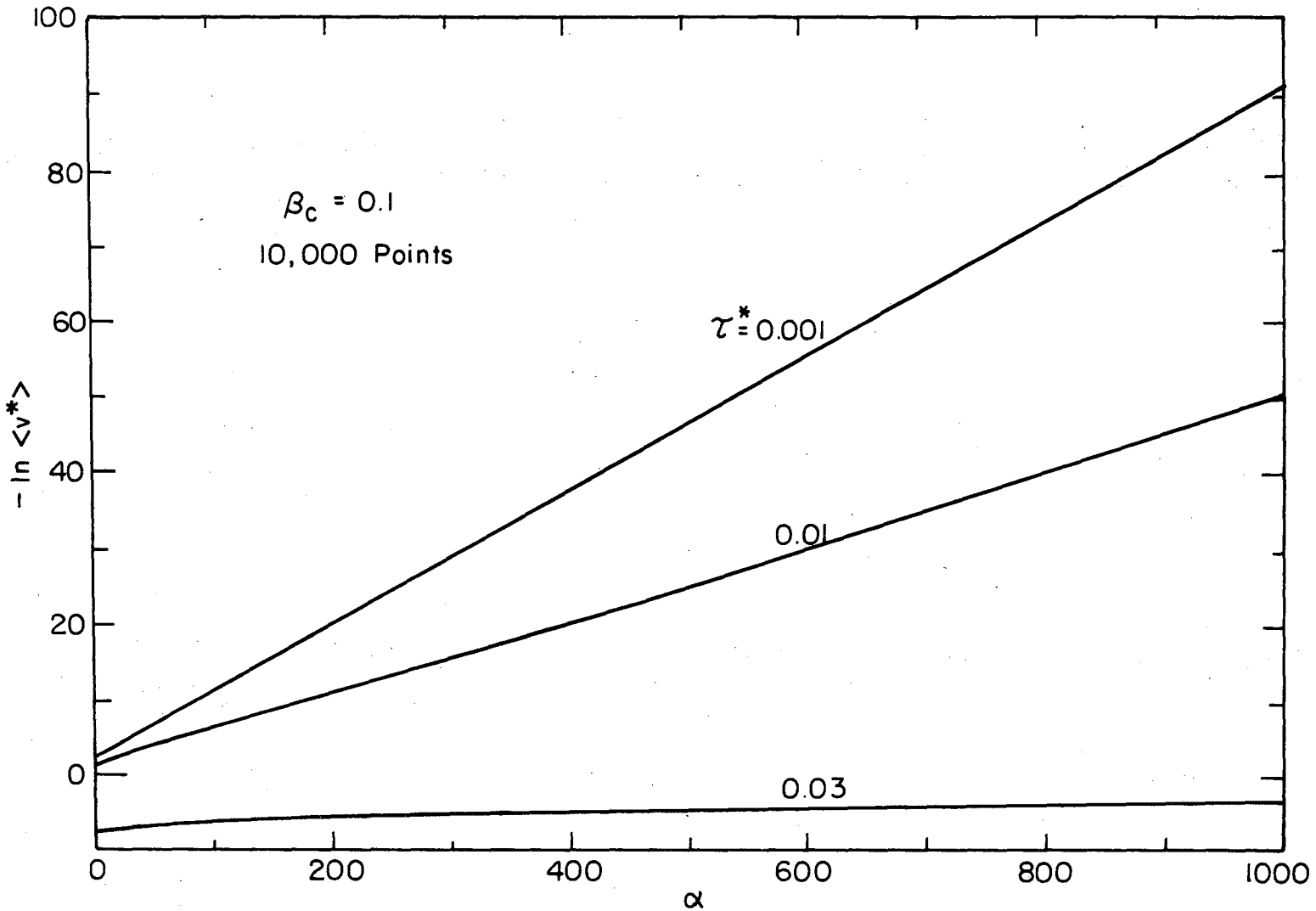

XBL754-6133

Fig. 5

0 0 0 0 4 3 0 5 3 1 1

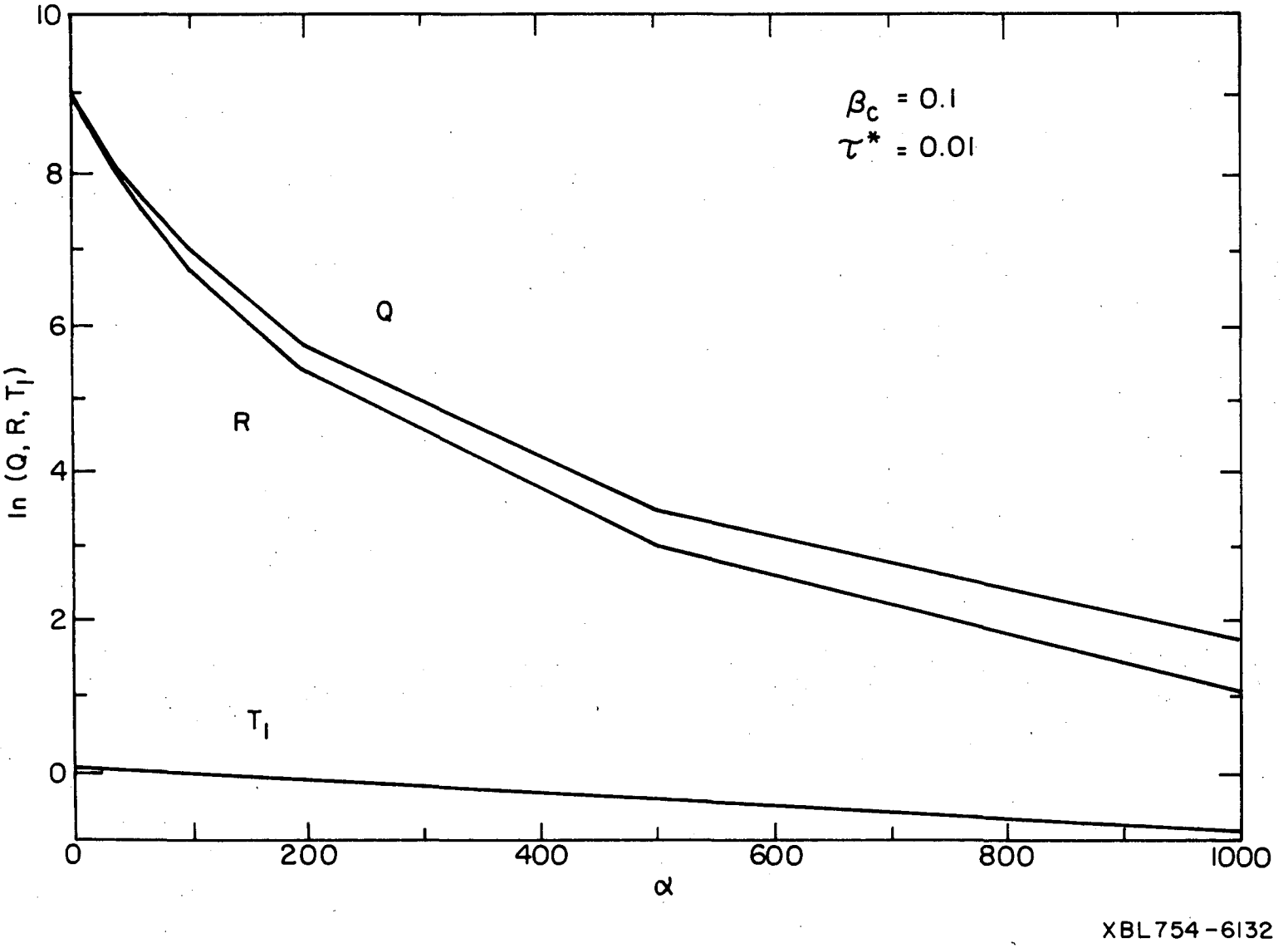
β_c = 0.1
τ^* = 0.01
Q
R
T_1
ln (Q, R, T_1)
α
10
8
6
4
2
0
0
200
400
600
800
1000
XBL754-6132

Fig. 6

0 0 0 4 3 0 5 3 1 2

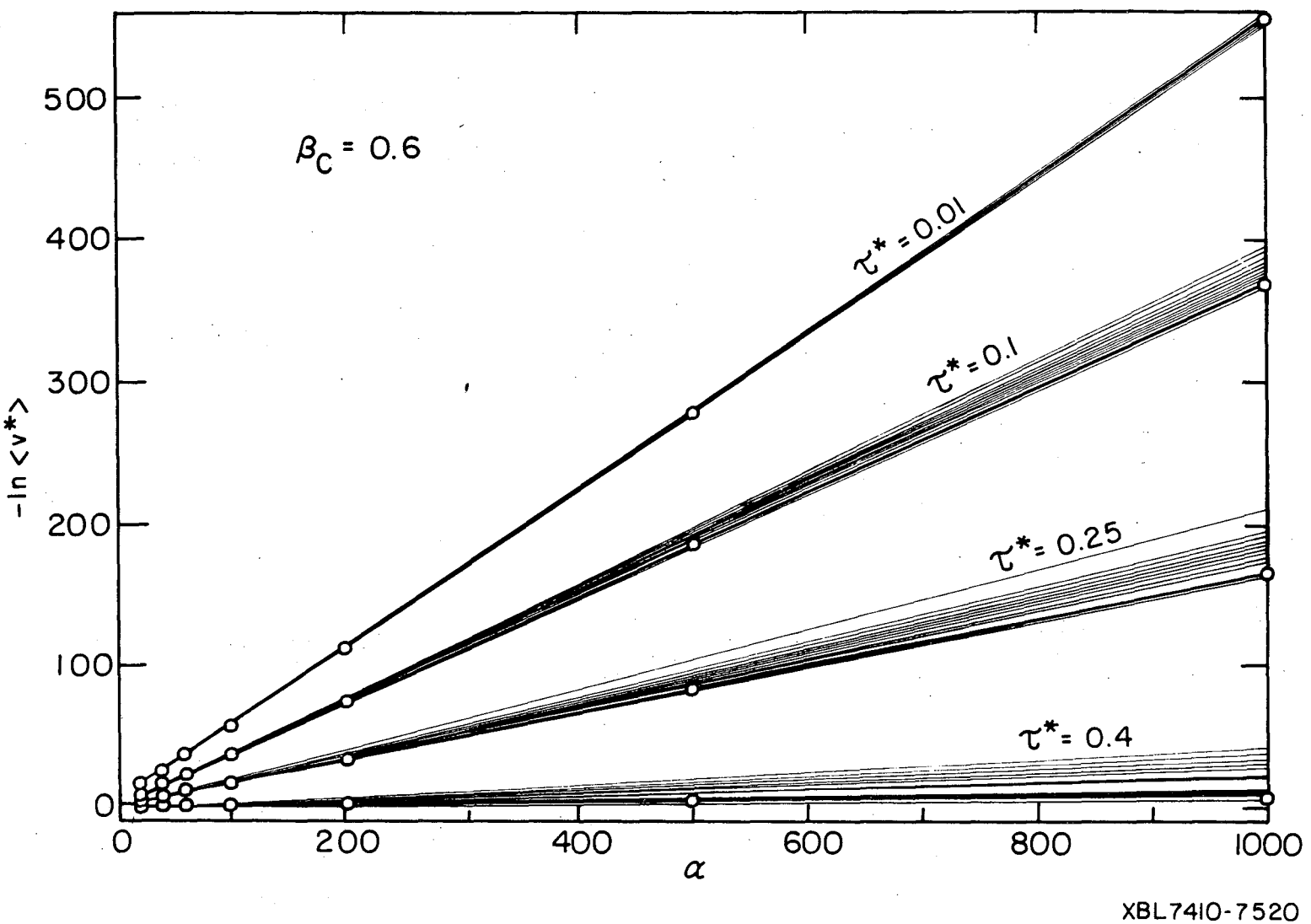

Fig. 7

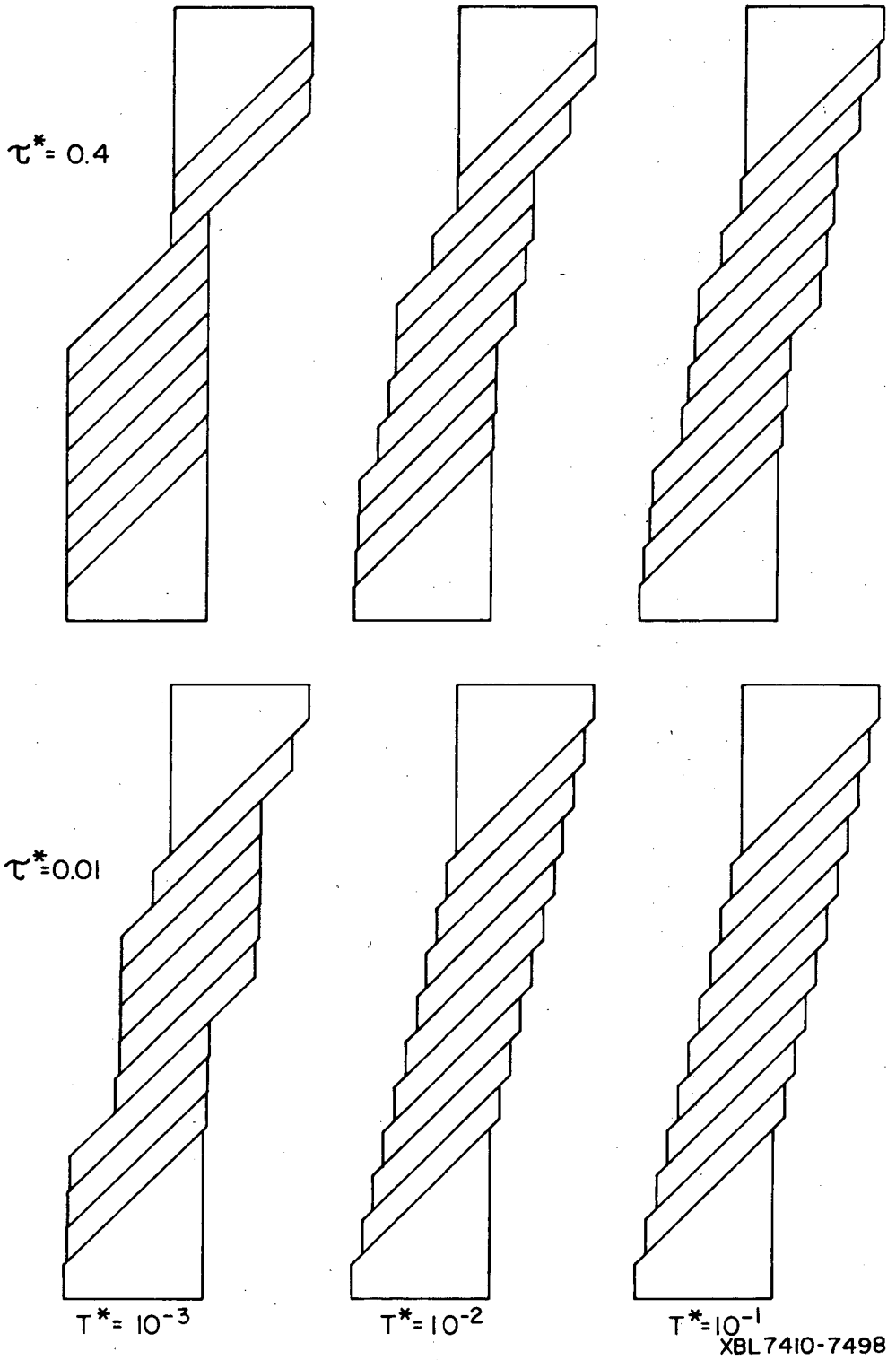

Fig. 8

0 0 0 0 4 3 0 5 3 1 3

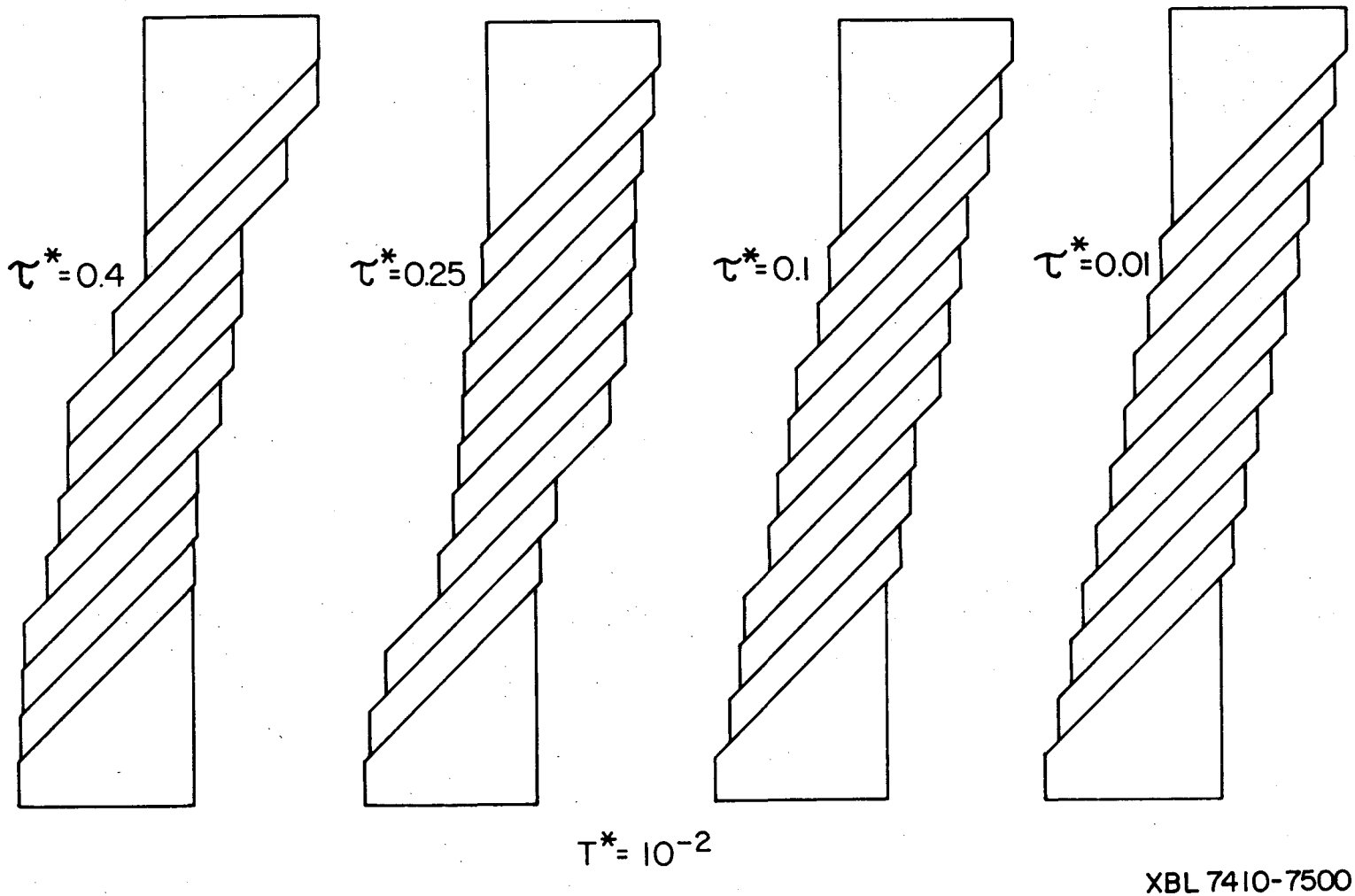

Fig. 9

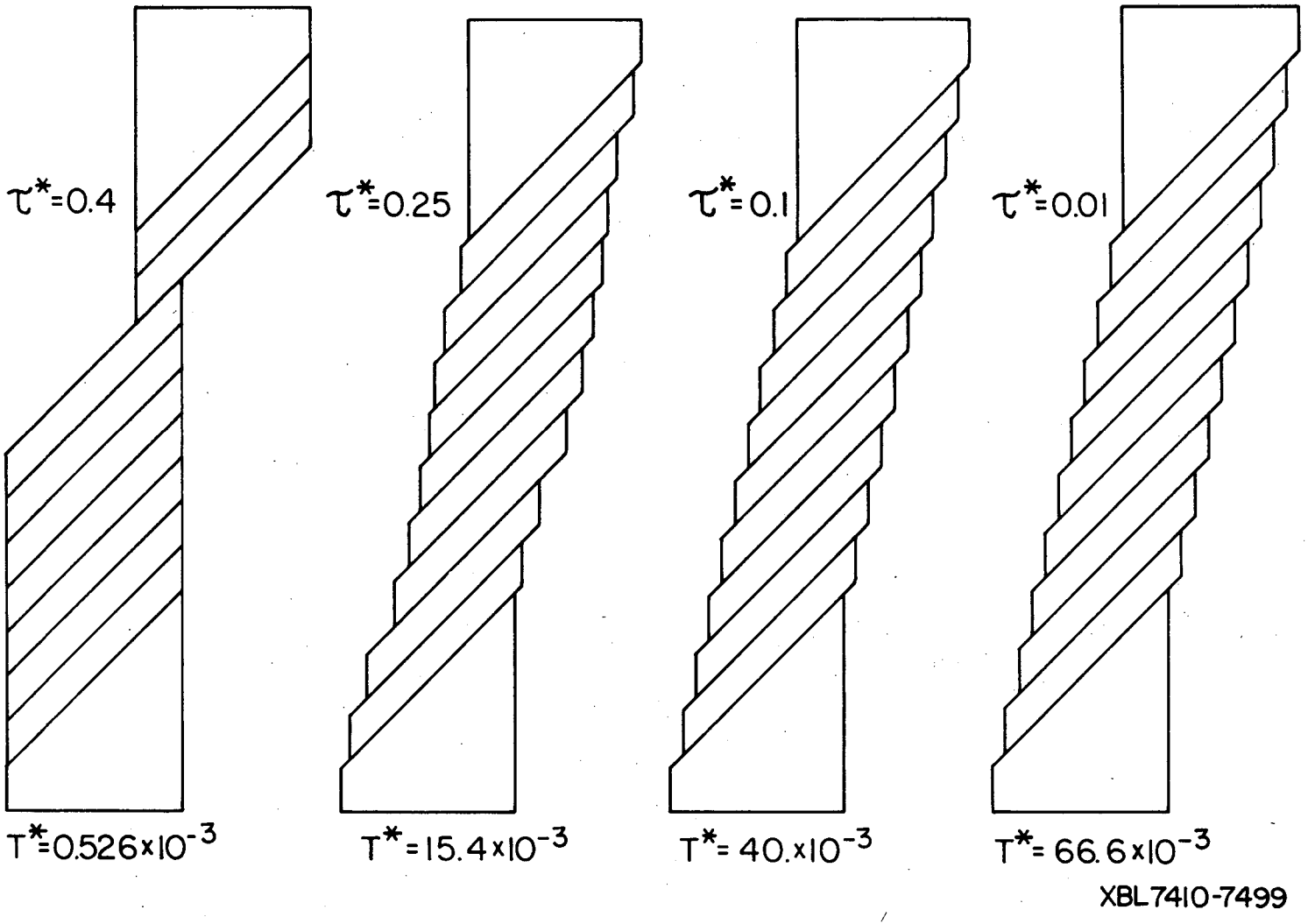
τ*=0.4
τ*=0.25
τ*=0.1
τ*=0.01
T*=0.526×10^-3
T*=15.4×10^-3
T*=40.×10^-3
T*=66.6×10^-3
XBL7410-7499

Fig. 10

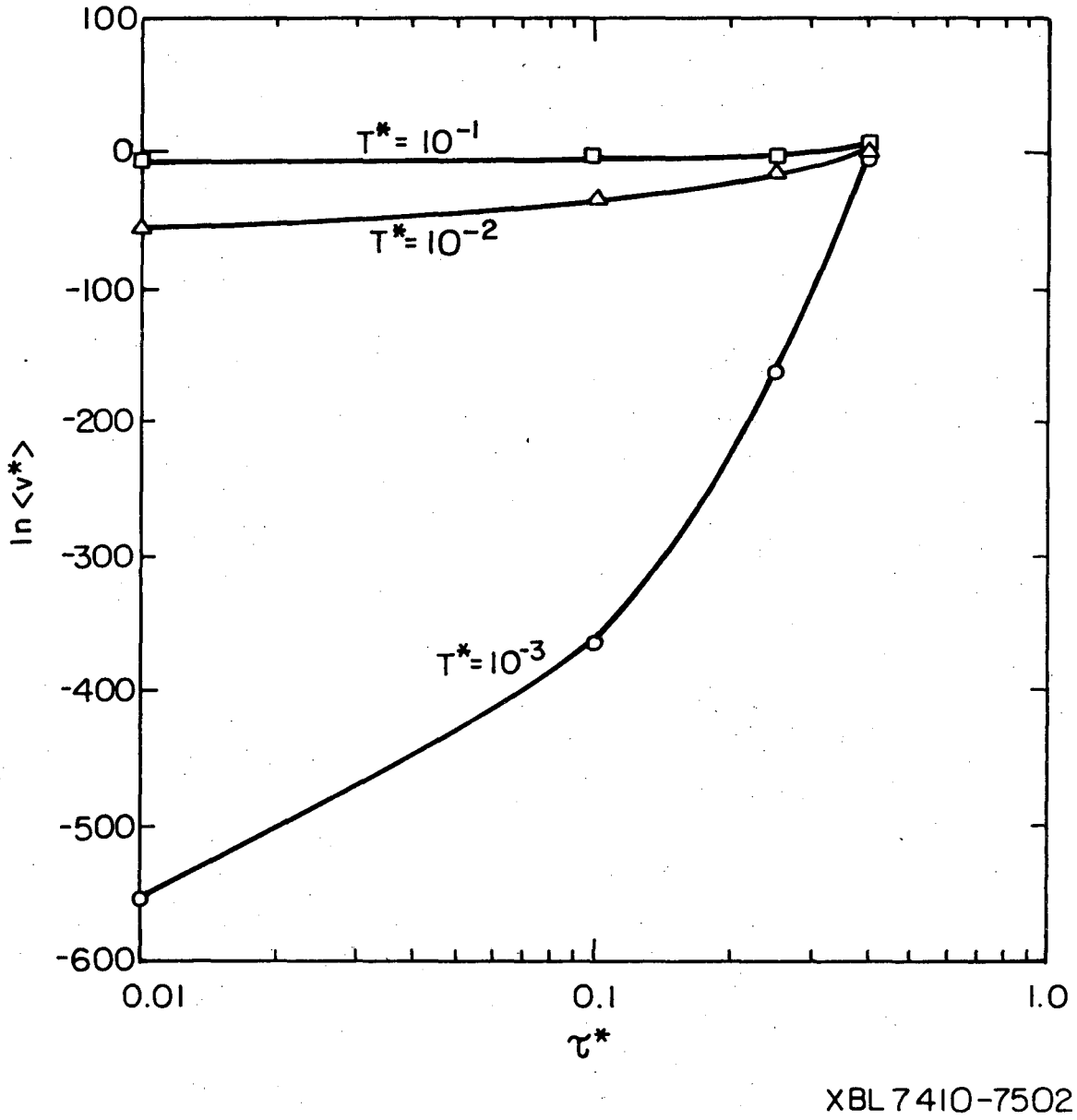
100
0
-100
-200
-300
-400
-500
-600
ln <v*>
T* = 10^-1
T* = 10^-2
T* = 10^-3
0.01
0.1
1.0
τ*
XBL 7410-7502

Fig. 11

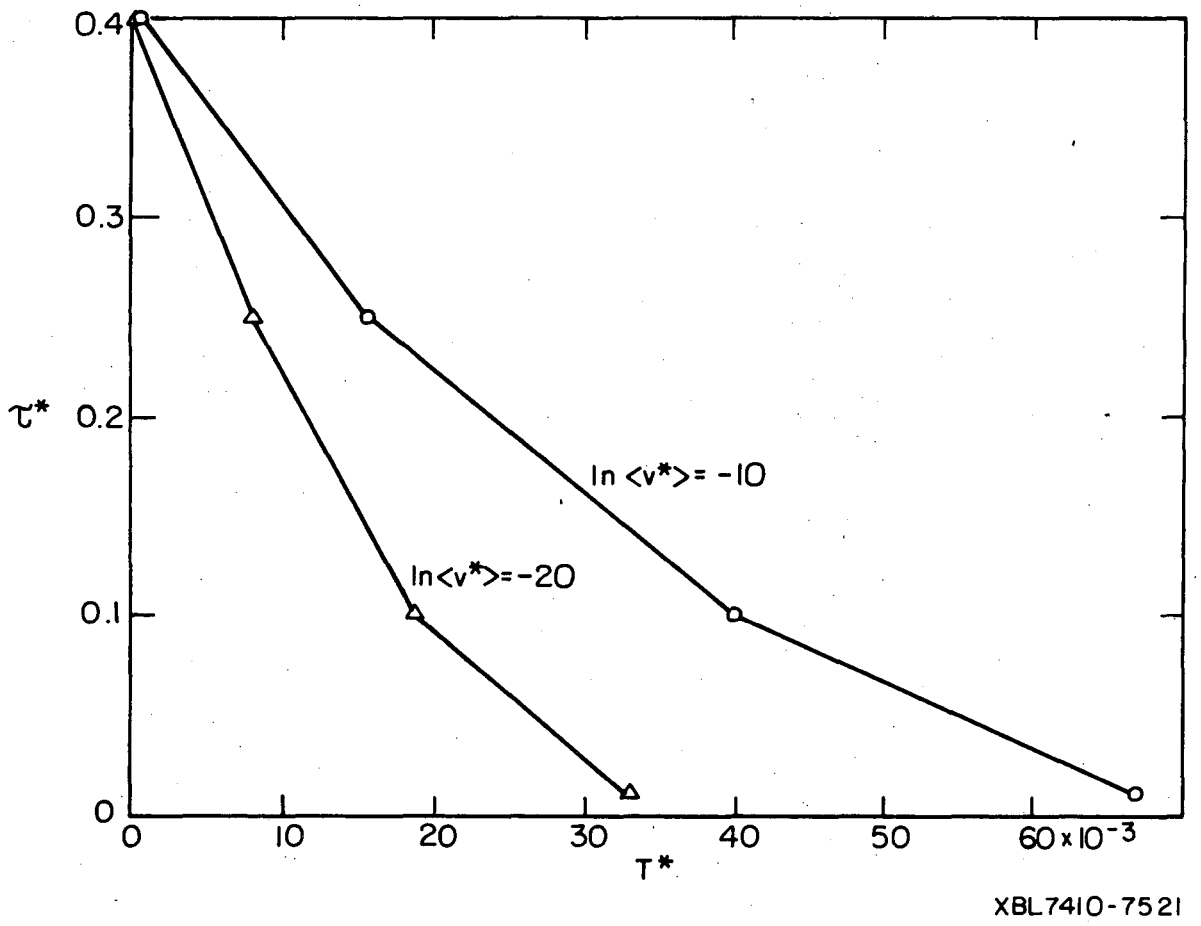

Fig. 12

0 0 0 0 4 3 0 5 3 1 5

LEGAL NOTICE

This report was prepared as an account of work sponsored by the United States Government. Neither the United States nor the United States Energy Research and Development Administration, nor any of their employees, nor any of their contractors, subcontractors, or their employees, makes any warranty, express or implied, or assumes any legal liability or responsibility for the accuracy, completeness or usefulness of any information, apparatus, product or process disclosed, or represents that its use would not infringe privately owned rights.

TECHNICAL INFORMATION DIVISION
LAWRENCE BERKELEY LABORATORY
UNIVERSITY OF CALIFORNIA
BERKELEY, CALIFORNIA 94720